CrossMark

An approach for detecting five typical vegetation types on the Chinese Loess Plateau using Landsat TM data

Zhi-Jie Wang · Ju-Ying Jiao · Bo Lei · Yuan Su

Abstract Remote sensing can provide large-scale spatial data for the detection of vegetation types. In this study, two shortwave infrared spectral bands (TM5 and TM7) and one visible spectral band (TM3) of Landsat 5 TM data were used to detect five typical vegetation types (communities dominated by *Bothriochloa ischaemum*, *Artemisia gmelinii*, *Hippophae rhamnoides*, *Robinia pseudoacacia*, and *Quercus liaotungensis*) using 270 field survey data in the Yanhe watershed on the Loess Plateau. The relationships between 200 field data points and their corresponding radiance reflectance were analyzed, and the equation termed the vegetation type index (VTI) was generated. The VTI values of five vegetation types were calculated, and the accuracy was tested using the remaining 70 field data points. The applicability of VTI was also tested by the distribution of vegetation type of two small watersheds in the Yanhe watershed and field sample data collected from other regions (Ziwuling Region, Huangling County, and Luochuan County) on the Loess Plateau. The results showed that the VTI can effectively detect the five vegetation types with an average accuracy exceeding 80 % and a representativeness above 85 %. As a new approach for monitoring vegetation types using remote sensing at a larger regional scale, VTI can play an important role in the assessment of vegetation restoration and in the investigation of the spatial distribution and community diversity of vegetation on the Loess Plateau.

Z.-J. Wang
College of Life Science, Guizhou University, Guiyang 550025
Guizhou Province, China

J.-Y. Jiao (✉) · Y. Su
Institute of Soil and Water Conservation, Northwest A&F
University, 26 Xinong Road, Yangling 712100 Shaanxi Province,
China
e-mail: jyjiao@ms.iswc.ac.cn

Z.-J. Wang · J.-Y. Jiao · B. Lei
State Key Laboratory of Soil Erosion and Dryland Farming on the
Loess Plateau, Institute of Soil and Water Conservation, Chinese
Academy of Sciences and Ministry of Water Resources,
26 Xinong Road, Yangling 712100 Shaanxi Province, China

Introduction

Vegetation not only forms essential habitats for plant and animal species but is also a prerequisite for ecosystem function. Vegetation provides many ecosystem services, principally through the protection of the land surface, the amelioration or modification of the local climate, the maintenance of critical ecosystem processes, and the conservation of biodiversity (Hölzel et al. 2012). Vegetation types represent different stages in vegetation restoration and succession and are closely related to soil properties, water runoff, soil erosion, as well as ecological stability (Jiao et al. 2008a, b; Nagase and Dunnett 2012; Qiu et al. 2010; Wang et al. 2011). Therefore, it is important to accurately detect vegetation types in ecological studies.

The traditional method for detecting vegetation types is to employ field investigations or polygon mapping (Wen et al. 2010). These methods involve intensive and time-consuming fieldwork and cannot be applied conveniently to large regions. Satellite imagery and remote sensing technology provide a practical and economical means for the study of vegetation at large spatial and temporal scales and are necessary to address this fundamental perspective (Elmore et al. 2000; Xie et al. 2008). Presently, several vegetation indices (VIs)/models using remote sensing methods have been developed to monitor vegetation types, such as a novel shape model developed using the two-step filtering (TSF) method for detecting the phenological stages of maize and soybeans (Sakamoto et al. 2010). The Poaceae abundance index (PAI) was developed to discriminate Poaceae grass at the field scale (Shimada et al. 2012), a niche model to monitor peat swamp forests was developed (Shimada et al. 2006), the simple geometric model (SGM) of the surface bidirectional reflectance distribution function (BRDF) to determine grass and shrub types was completed (Chopping et al. 2003), and the greenness spectral vegetation indices (SVIs) for the classification of semi-arid shrub types were also developed (Duncan et al. 1993). However, most of these VIs/models have many parameters related to ground-based measurements of spectral data and still cannot guarantee the prediction accuracy for the biophysical and biochemical variables of the vegetation canopy (Shimada et al. 2012).

Moreover, most of these VIs were near-infrared (NIR)- and red-based indices and they have several limitations in their sensitivity due to the soil background, atmospheric influence, and/or the saturation of index values in the case of dense and multi-layered canopies (Karnieli et al. 2001). Many studies have been conducted to minimize those limitations, and three ways of doing so have emerged. The first method incorporates a canopy background adjustment factor to minimize background influence (Huete 1988; Major et al. 1990; Qi et al. 1994). The second method directly corrects the red radiance for the aerosol effect by incorporating the blue (B) band (Kaufman and Tanre 1992). Third, the shortwave infrared spectral bands (1.6 and 2.1 μm) for the remote sensing of the surface cover in the absence of aerosol effects have been used to construct VIs in recent studies (Kaufman et al. 1997). Several studies have shown that the 1.55- to 1.75-μm spectral interval is the best-suited band in the 0.7- to 2.5-μm region for monitoring plant canopy water status (Tucker 1980). The 1.6-μm region is the most sensitive to vegetation senescence (Qi et al. 2000), and the 2.1-μm band is more similar to the 0.66-μm band in its dependence on surface cover than the 1.24- or 1.6-μm bands and has the potential to better mimic the normalized difference vegetation index (NDVI) without aerosol interference (Karnieli et al. 2001; Kaufman et al. 1997). All of these studies have provided important reference points for developing new VIs to detect vegetation signals.

The Chinese Loess Plateau is considered one of the most severely eroded areas in the world (Wang et al. 2011). Accelerated erosion has been a constant threat to the livelihoods of rural families and is a large problem for the ecosystem and the environment (van den Elsen et al. 2003). For the aim of controlling soil and water losses and improving the ecological environment in the area, the Chinese Central Government has issued the "Grain for Green" policy for the restoration of vegetation on the Loess Plateau since 1999. As part of this policy, croplands (especially slope lands) have been extensively shifted to forest lands and grasslands (Jiao et al. 2008a, b; Wang et al. 2011). The vegetation landscape on the Loess Plateau includes natural secondary vegetation types and afforestation types. The distribution, scale, and restoration effect of different vegetation types are quite significant for the assessment of the environmental effect of revegetation, decision-making for ecological environment construction and soil and water conservation on the Loess Plateau, and the analysis of runoff and sediment variation in the Yellow River. However, no corresponding VIs have been developed to monitor vegetation types in the Loess Plateau region.

In this study, we attempted to develop a new method, termed the vegetation type index (VTI), to discriminate the typical vegetation types in the Yanhe watershed on the Loess Plateau from Landsat TM images and field survey data. Our aims were to offer a new method for remote detection of vegetation types and their spatial distribution at a larger regional scale and then to provide a basis for the assessment of revegetation effects and vegetation diversity in the Loess Plateau region.

Materials and methods

Study area

The Yanhe watershed (36° 23′–37° 17′ N, 108° 45′–110° 28′ E) is located in the central part of the Loess

Plateau and in the middle reaches of the Yellow River (Fig. 1). The watershed has a warm, temperate continental monsoon climate with distinct wet and dry seasons. The mean annual precipitation is 497 mm (1970–2000, Cv 22 %), of which more than 65 % falls from July to September. The annual average temperature varies from 8.8 to 10.2 °C. The annual reference evapotranspiration is approximately 1000 mm. The topography, soil type, and land use patterns of the Yanhe watershed are typical of the Loess Plateau (Jiao et al. 2011; Su et al. 2012). The original tree and shrub vegetation was removed long ago through human activities. The natural secondary *Quercus liaotungensis* forest, as the climax community of vegetation succession, is only distributed in the southern part of the Yanhe watershed and is accompanied by *Acer ginnala*, *Platycladus orientalis*, *Populus simonii*, and *Ulmus pumila* species. The main planted trees and shrubs widely dispersed in this region are *Robinia pseudoacacia*, *P. simonii*, *Caragana microphylla*, and *Hippophae rhamnoides*. Grass species such as *Bothriochloa ischaemum*, *Stipa bungeana*, *Lespedeza davurica*, *Cleistogenes chinensis*, and *Artemisia gmelinii* can be found widely in field

edges, abandoned lands, and gully slopes (Jiao et al. 2008a, b; Wang et al. 2011).

Data collection and analysis

Figure 2 shows the technical process of VTI building. Two data sets, the Landsat 5 TM image data and the field vegetation type sampling data, were collected to generate the VTI equation and to test its accuracy for the detection of vegetation types in the Yanhe watershed. The TM image data sets were used to provide each vegetation type's reflectance value in different spectral bands. Field sampling data of vegetation types combined with the corresponding reflectance values were used to analyze the relationship between the spectral characteristics of the TM bands and vegetation types to build the VTI equation and to test its accuracy.

Image data

Two Landsat Thematic Mapper images were acquired on June 17, 2010 (Table 1). The Landsat TM sensor had six visible-infrared bands (pixel size 30 m×30 m) and
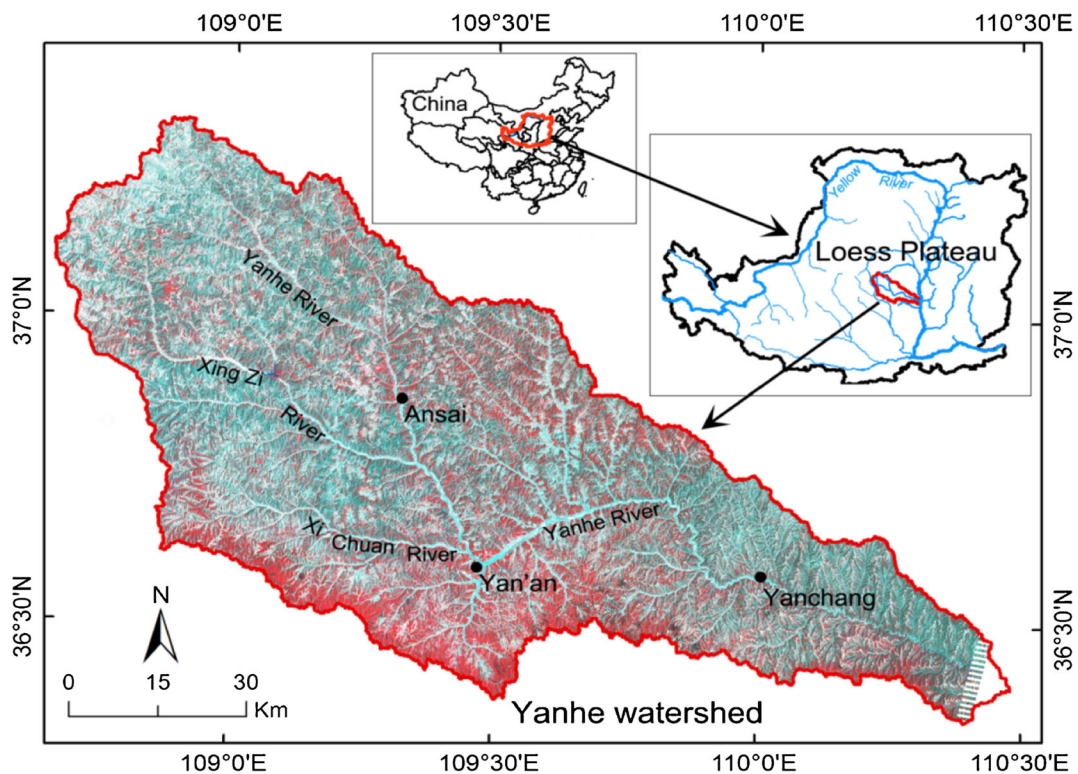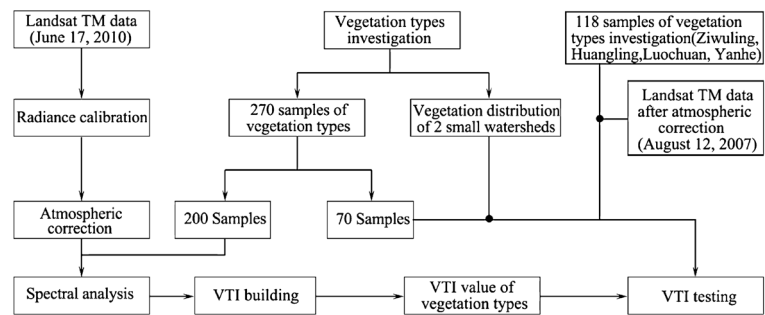

Fig. 1 Location of the Yanhe watershed on the Loess Plateau, China

Fig. 2 The technical process of VTI building

one thermal band (pixel size 120 m×120 m). Images of the Yanhe watershed were taken from path 127 and rows 35 to 36. All images were selected from cloud-free scenes during the summer (June 17) of 2010.

Field investigation data of vegetation types

Several studies in the area have indicated that both *B. ischaemum*-dominated and *A. gmelinii*-dominated communities are the main grass types in the mid-later succession stages extensively distributed in the abandoned cropland and gully slopes (Jia et al. 2011; Jiao et al. 2008a, b). *Q. liaotungensis* dominates the natural secondary forest and is the climax community of vegetation succession distributed in the southern part of the Yanhe watershed (Wang et al. 2011). *R. pseudoacacia* and *H. rhamnoides* have long been planted over vast regions for soil and water conservation, especially during the Grain for Green period (Li et al. 1996; Qiu et al. 2010; Wang et al. 2011). Therefore, we selected these five typical vegetation types to build the VTI.

A total of 270 field samples (2 m×2 m for grass quadrant size, 5 m×5 m for shrub quadrant size, and 10 m×10 m for tree quadrant size) were collected during the 2009 and 2012 growing seasons (Fig. 3). The community composition and the dominated species of each

sample site were investigated. Finally, The *B. ischaemum*-dominated community (*Bi*) had 55 samples, the *A. gmelinii*-dominated community (*Ag*) had 55 samples, the *H. rhamnoides*-dominated community (*Hr*) had 53 samples, the *R. pseudoacacia*-dominated community (*Rp*) had 54 samples, and the *Q. liaotungensis*-dominated community (*Ql*) had 53 samples. Then, 200 samples (40 samples of each type) were randomly selected to analyze the relationship between the reflectance value of the spectral bands and the five vegetation types, generate the VTI equation, and protocol the VTI values of the vegetation types. The other 70 samples were used to test the accuracy of the VTI.

Meanwhile, vegetation type distribution maps of the Chenjiagua watershed, in the forest-steppe zone, and the Shanghenian watershed, in the forest zone (Fig. 3), were mapped based on the field survey of June 2012 and were then used to test the applicability of the VTI.

VTI building

Image data pre-processing

Two processing steps were completed for the two Landsat TM images: (1) radiometric calibration and

Table 1 Image information of the Yanhe watershed and spectral characteristics of the TM sensor

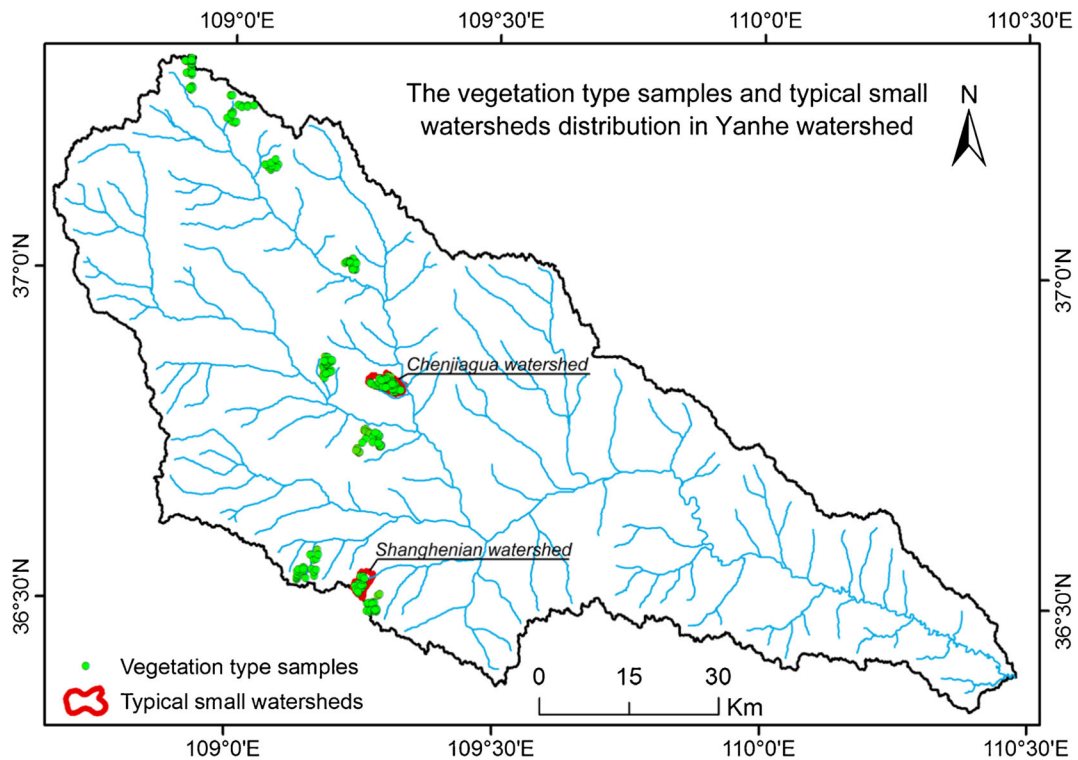| Path	Row	Acquisition date	Sun azimuth	Sun elevation	Cell size (m)	Band	Spectral range (μm)
127	35	June 17, 2010	115.527	66.087	30	Blue (TM1)	0.45–0.52
						Green (TM2)	0.52–0.60
						Red (TM3)	0.63–0.69
127	34	June 17, 2010	118.836	65.66	30	Near-IR (TM4)	0.76–0.90
						Shortwave infrared (TM5)	1.55–1.75
						Shortwave infrared (TM7)	2.08–2.35

Fig. 3 The distribution vegetation type samples and typical small watersheds in the Yanhe watershed

(2) atmospheric correction. These two steps were performed using the ENVI 4.7 software.

Radiometric calibration Radiometric calibration allows the full Landsat data set to be used in a quantitative sense (Thorne et al. 1997). The Landsat calibration converts the digital number (DN) with a range between 0 and 255 to radiance values (Wm^{-2} sr^{-1} μm^{-1}). In this study, the *bias* and *gain* (or *offset*) values (Table 2) from the header files were used in the calibration. The formula to convert DN to radiance using gain and bias (offset) values is as follows:

$$L_\lambda = \text{Gain} \times \text{DN} + \text{Offset} \qquad (1)$$

where L_λ is the cell value as radiance, DN is the cell value as digital number, gain is the gain value for a specific band (Wm^{-2} sr^{-1} μm^{-1} DN^{-1}), and offset is the bias value for a specific band (Wm^{-2} sr^{-1} μm^{-1}).

Atmospheric correction Remotely sensed images include information about the atmosphere and the Earth's surface, so removing the influence of the atmosphere is a critical pre-processing step (Solutions 2009).

To accurately compensate for atmospheric effects, the Fast Line-of-sight Atmospheric Analysis of Spectral Hypercubes (FLAASH) correction modeling tool was used. FLAASH employs atmospheric correction based on MODTRAN 4 radiative transfer models and corrects for absorptions by atmospheric water vapor, methane, oxygen, carbon dioxide, and ozone on a pixel-by-pixel basis (Adler-Golden et al. 1999; Carter et al. 2009). Several model parameters were set in the FLAASH correction module (Table 3).

Spectral analysis

The spectral characteristics in the different wavelengths of the five vegetation types from the six visible-infrared bands are demonstrated in Fig. 4. This indicated that the reflectance difference of the five vegetation types on each band was more obvious after atmospheric correction than the original TM images. However, for the spectral characteristics of the five vegetation types after atmospheric correction, the TM1 and TM2 bands could not distinguish the *Ag*, *Hr*, or *Ql* as they all have similar spectral signatures and the TM4 band could not

Table 2 Central wavelength, *gain*, and *offset* of Landsat TM5 (Chander et al. 2009)

Band	Central wavelength (μm)	Gain (Wm^{-2} sr^{-1} μm^{-1} DN^{-1})	Offset (Wm^{-2} sr^{-1} μm^{-1})
TM1	0.485	0.762824	−1.52
TM2	0.569	1.442510	−2.84
TM3	0.660	1.039880	−1.17
TM4	0.840	0.872588	−1.51
TM5	1.676	0.119882	−0.37
TM6	11.435	0.055158	1.24
TM7	2.223	0.065294	−1.15

distinguish the *Bi*, *Hr*, and *Ag* ($p > 0.05$). However, the TM3, TM5, and TM7 bands have greater differences in the five types compared to the other bands. Furthermore, previous studies have shown that the TM3 band (0.63 to 0.69 μm) is absorbed by chlorophyll and the TM5 and TM7 bands are absorbed by leaf water content with little being transmitted or reflected (Jackson 1984; Jensen 2006). The five vegetation types in this study have significant differences between each other in terms of chlorophyll and leaf water content ($p < 0.05$) (An and ShangGuan 2007; Jin et al. 2008). In theory, these five vegetation types could be discriminated using TM3, TM5, and TM7.

Scatter plots of the TM5 band vs. the TM3 band and the TM5 band vs. the TM7 band of the five vegetation types are presented in Figs. 5 and 6, respectively. The reflectance value could be clearly distinguished between different vegetation types. From the ANOVA analysis (Table 4), there are significant differences among the five vegetation types ($p < 0.05$), except for *Rp* and *Hr* in TM5 ($p = 0.662$). The results indicate that the TM3, TM5, and TM7 bands could potentially detect the vegetation types.

Previous studies have reported that the image ratio operation could enhance and distinguish the ground features that had the largest different spectrum characteristic in different bands, minimize differences in illumination conditions, and eliminate the radiation changes caused by slopes and aspects (Sabins 1987). Therefore, the ratio operation was priority selected to develop the VTI equation. Based on the relationship of the spectral characteristics of the five vegetation types among the above-selected bands, we tried multiple combinations of TM3, TM5, and TM7. Finally, following the simplicity of NDVI and DVI, the VTI was defined as follows:

$$\text{VTI} = \frac{L_{\text{TM5}} - L_{\text{TM3}}}{L_{\text{TM5}} + L_{\text{TM3}}} + \frac{L_{\text{TM5}}}{L_{\text{TM7}}} \tag{2}$$

where L_{TM5}, L_{TM3}, and L_{TM7} are the reflectance of the TM5, TM3, and TM7 bands, respectively.

VTI testing

To confirm the suitability and accuracy of VTI, 70 testing samples that were not involved in generating the VTI equation were used to test the accuracy of VTI using the error matrix method

Table 3 Several major settings of the FLAASH correction model

| Model/parameters	Model setting	Description
Atmosphere model	Mid-latitude summer (MLS)	The season and latitude of the image data in the present study belong to MLS
Aerosol model	Rural	Aerosols in study area are not strongly affected by urban or industrial sources
Initial visibility	40 km	The weather in the image was clear
Aerosol retrieval	Kaufman-Tanre (K-T)	KT upper channel was set as band 7 (2.2200 μm), and KT lower channel was set as band 3 (0.6600 μm)
Maximum upper channel reflectance	0.10	Defaults
Reflectance ratio	0.45	Defaults
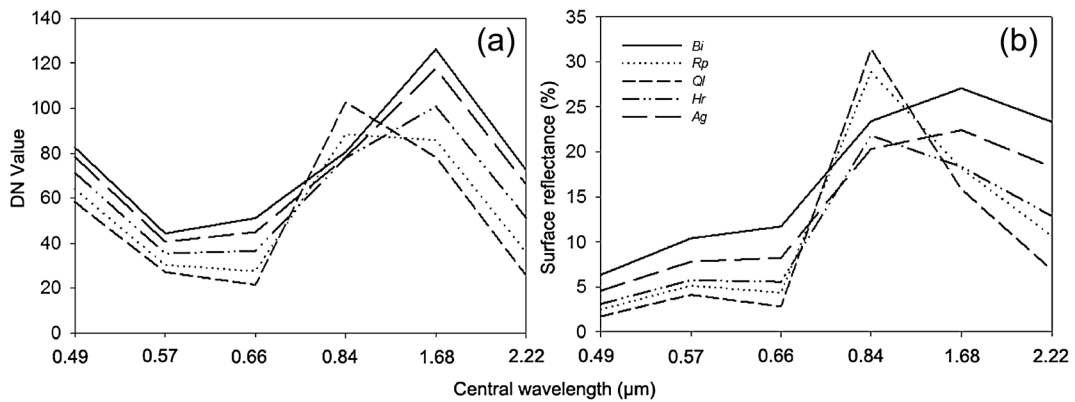
Fig. 4 Spectrum characteristics of the five vegetation types in different TM bands. *a* The spectrum characteristic of the original TM image. *b* The spectrum characteristics of the image after atmospheric correction. *Bi* is *B. ischaemum*-dominated community, *Ag* is *A. gmelinii*-dominated community, *Hr* is *H. rhamnoides*-dominated community, *Rp* is *R. pseudoacacia*-dominated community, and *Ql* is *Q. liaotungensis*-dominated community

(Congalton 1991). The accuracy criteria for detecting vegetation types were set as 85 % minimum overall and 70 % per type (Thomlinson et al. 1999). Two small watersheds (the Chenjiagua watershed in a forest-steppe zone and the Shanghenian watershed in a forest zone) were used to test the applicability of VTI using the kappa index method (Congalton 1991) based on the field investigation of vegetation types in June 2012.

To test the applicability of VTI in different Landsat image data and other regions on the Loess Plateau, the Landsat 5 TM data set (path 127, row 34), which was acquired on August 12, 2007, and a total of 118 field samples on the Loess Plateau were collected to test the accuracy of VTI using the confusion matrix method and the kappa index method. In the 118 field samples, there were 25 samples for *Bi*, 30 samples for *Ag*, and 19 samples for *Hr* in Yanhe watershed investigated by our team in 2006 and 27 samples for *Rp* in the Ziwuling Region, Huangling County, and Luochuan County reported by Chen et al. (2014)
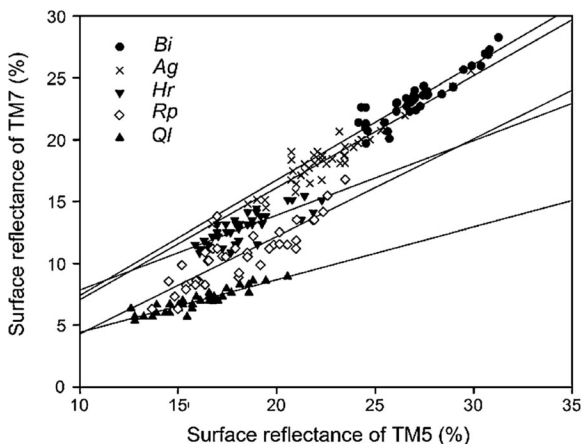

Fig. 5 The relationship of radiance reflectance between TM5 and TM7. *Bi* is *B. ischaemum*-dominated community, *Ag* is *A. gmelinii*-dominated community, *Hr* is *H. rhamnoides*-dominated community, *Rp* is *R. pseudoacacia*-dominated community, and *Ql* is *Q. liaotungensis*-dominated community

Fig. 6 The relationship of radiance reflectance between TM5 and TM3. *Bi* is *B. ischaemum*-dominated community, *Ag* is *A. gmelinii*-dominated community, *Hr* is *H. rhamnoides*-dominated community, *Rp* is *R. pseudoacacia*-dominated community, and *Ql* is *Q. liaotungensis*-dominated community
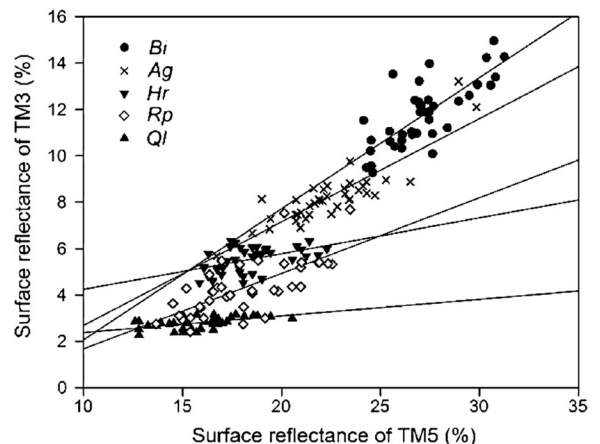
Table 4 ANOVA analysis of different vegetation types in the selected spectral bands

	Sum of squares	df	Mean square	F	Sig.
TM3					
Between groups	19,870,000.00	4	4,968,091.28	458.862	0.000[a]
Within groups	2,111,261.65	195	10,826.98		
Total	21,980,000.00	199			
TM5					
Between groups	31,513,620.23	4	7,878,405.06	170.976	0.000[a]
Within groups	8,985,389.93	195	46,078.92		
Total	40,500,000.00	199			
TM7					
Between groups	67,070,000.00	4	16,770,000.00	478.314	0.000[a]
Within groups	6,835,895.93	195	35,055.88		
Total	73,910,000.00	199			

[a] The mean difference is significant at the $p < 0.05$ level

and 17 samples for Ql in the Ziwuling Region reported by An and ShangGuan (2007).

Comparison of VTI with NDVI and supervised classification

NDVI is the most widely used vegetation index and is a commonly used indicator of vegetation parameters such as vegetation abundance, leaf area index (LAI), and the fraction of photosynthetically active radiation (Elmore et al. 2000; Karnieli et al. 2001). However, NDVI has some defects in vegetation parameter monitoring. For example, it is more sensitive to sparse vegetation densities, but is less sensitive to high vegetation densities; it is not always comparable across a heterogeneous scene (Elmore et al. 2000; Jackson and Huete 1991). To determine if VTI could overcome these disadvantages of NDVI, VTI was compared to NDVI. For comparison, the NDVI of the Chenjiagua and Shanghenian watersheds was calculated and then the classification accuracy of the five vegetation types using NDVI was tested with the kappa index method using the same accuracy criteria as for the VTI. A Z test was used to test the sensitivities of NDVI and VTI to detect vegetation community types.

The supervised classification of maximum likelihood classifiers (MLCs) is widely used in classifying remotely sensed data for its high precision and accuracy (Dean and Smith 2003; Manandhar et al. 2009; Yang et al. 2011). To test if VTI could obtain satisfactory accuracy for the detection of five vegetation types like MLC, the supervised classification using MLC methods of the Chenjiagua and Shanghenian watersheds was processed. The classification accuracy of the five vegetation types using MLC was also tested with the kappa index method.

Results

The VTI values of the vegetation types

The VTI values of the five vegetation types with 200 samples according to Eq. (2) are demonstrated in Fig. 7. The VTI value of each type was calculated according to the accuracy criteria in which the detection of vegetation types was greater than 85 % minimum overall and 70 % per type (Thomlinson et al. 1999). The values ranged from 1.48 to 1.60 for Bi, from 1.60 to 1.80 for Ag, from 1.80 to 2.00 for Hr, from 2.00 to 2.80 for Rp, and above 2.80 for Rp. Statistically, the VTI value of all five vegetation types had significant differences between each other at the 99 % confidence level based on the least significance difference (LSD) test ($p < 0.01$) (Table 5). The representativeness of each type was above 85 %, except for Hr, which was 75 %.
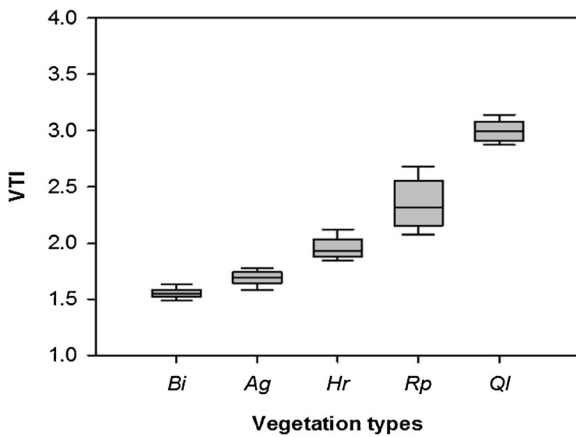
Fig. 7 VTI of the five vegetation types (mean±SD). *Bi* is *B. ischaemum*-dominated community, *Ag* is *A. gmelinii*-dominated community, *Hr* is *H. rhamnoides*-dominated community, *Rp* is *R. pseudoacacia*-dominated community, and *Ql* is *Q. liaotungensis*-dominated community

The VTI accuracy test

Table 6 shows the vegetation classification accuracy using a confusion matrix. The accuracy of all vegetation types exceeded 70 %, and the average accuracy was 80 %. The *Bi* had a lower accuracy than the other four types due to confusion with *Ag*. *Hr* and *Rp* also displayed the confusion phenomena in the Landsat TM data set to some extent.

VTI applicability test

To illustrate the applicability of the VTI, the vegetation distribution in the Chenjiagua small watershed in the forest-steppe zone and the Shanghenian small watershed

Table 6 Confusion matrix of VTI values between different vegetation types

	Bi	*Ag*	*Hr*	*Rp*	*Ql*	Sample number	Accuracy (%)
Bi	11	4	0	0	0	15	73.33
Ag	2	12	0	1	0	15	80.00
Hr	0	0	12	1	0	13	92.31
Rp	0	0	2	11	1	14	78.57
Ql	0	0	0	3	10	13	76.92

n=70; *Bi* is *B. ischaemum*-dominated community, *Ag* is *A. gmelinii*-dominated community, *Hr* is *H. rhamnoides*-dominated community, *Rp* is *R. pseudoacacia*-dominated community, and *Ql* is *Q. liaotungensis*-dominated community

in the forest zone of the Yanhe watershed was mapped using the VTI equation and the field survey (Figs. 8 and 9). The accuracy of the vegetation distribution maps was then validated using an error matrix and the kappa coefficient method (Table 7). The overall accuracy was 87.16 % in the Chenjiagua watershed and 88.73 % in the Shanghenian watershed. The kappa index of the five vegetation types in the two small watersheds exceeded 0.75, with the exception of 0.73 for *Ag* in the Chenjiagua watershed (Fig. 10); the overall kappa statistics of the two small watersheds reached above 0.80. This result indicates that the VTI reliably detected the vegetation types of the Yanhe watershed.

The accuracy of the VTI applied at the different dates of the Landsat data set was not used to build the VTI equation and other regions outside of the Yanhe watershed, as shown in Table 8. The overall accuracy of five vegetation types exceeded 80 % with the overall kappa

Table 5 The VTI value range and its accuracy for different vegetation types

Vegetation type	Value range of VTI	Representativeness (%)	Sample number
Bi	1.48–1.60a	85.0	40
Ag	1.60–1.80b	90.0	40
Hr	1.80–2.00c	75.0	40
Rp	2.00–2.80d	90.0	40
Ql	>2.80e	95.0	40
Overall representativeness	87.00 %	Total sample number	200

Bi is *B. ischaemum*-dominated community, *Ag* is *A. gmelinii*-dominated community, *Hr* is *H. rhamnoides*-dominated community, *Rp* is *R. pseudoacacia*-dominated community, and *Ql* is *Q. liaotungensis*-dominated community. The same letters in the same column indicate no significant differences between the measures, and different letters indicate significant differences between the measures based on the LSD test ($p<0.01$)
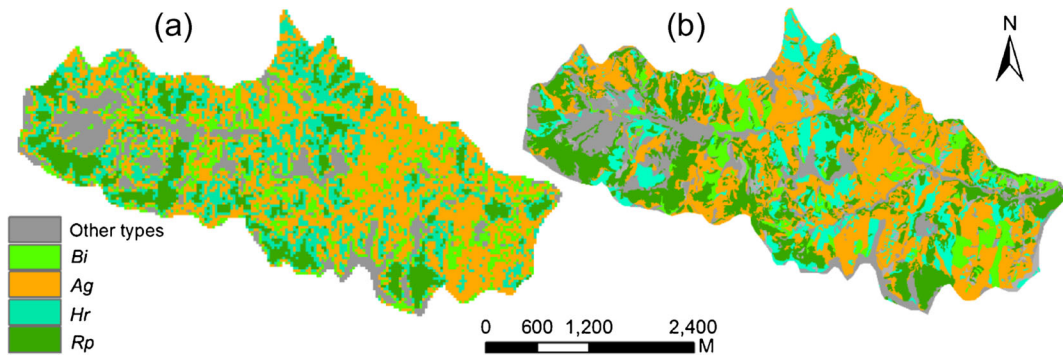
Fig. 8 Vegetation distribution map of the Chenjiagua watershed in the forest-steppe zone. *a* Calculated by the VTI. *b* Mapped by field survey. *Bi* is *B. ischaemum*-dominated community, *Ag* is *A. gmelinii*-dominated community, *Hr* is *H. rhamnoides*-dominated community, *Rp* is *R. pseudoacacia*-dominated community, and *Ql* is *Q. liaotungensis*-dominated community

statistics reached above 0.80. This indicated that the VTI could also be used in other places on the Loess Plateau or on other date-time Landsat data sets due to satisfactory classification accuracy.

Comparison of VTI with NDVI and supervised classification

The classification accuracy for the detection of the five vegetation types from NDVI maps was assessed using the kappa coefficient method (Table 9). The kappa index in the Chenjiagua watershed was below 0.6 for *Bi* and *Hr* and exceeded 0.6 for *Ag* and *Rp*. However, the

overall classification accuracy was only 69.86 % and the overall kappa statistic was in substantial agreement with the value of 0.6111. For the Shanghenian watershed, the kappa index of all five vegetation types was in slight agreement with the value below 0.2 and the overall classification and kappa statistics were only 24.72 % and 0.0821, respectively. Comparing the accuracy in the detection of the five vegetation types between NDVI and VTI indicated that NDVI had had a lower accuracy than VTI developed in this study for the detection of vegetation types and was ineffectively used to monitor the vegetation type. Moreover, Table 10 also shows that the VTI could detect the five vegetation community
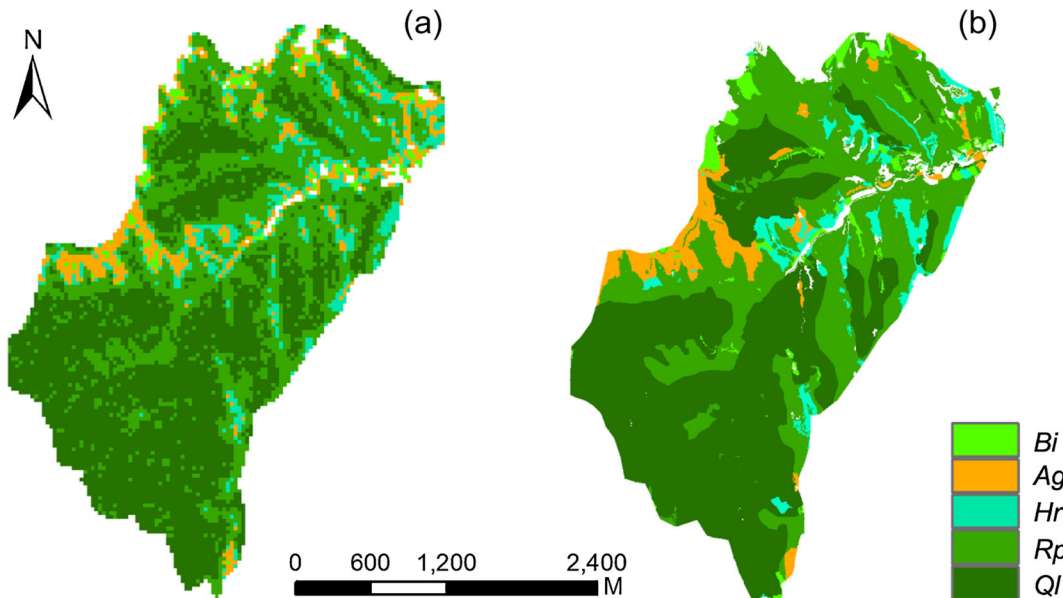

Fig. 9 Vegetation distribution map of the Shanghenian watershed in the forest zone. *a* Calculated by the VTI. *b* Mapped by field survey. *Bi* is *B. ischaemum*-dominated community, *Ag* is *A. gmelinii*-dominated community, *Hr* is *H. rhamnoides*-dominated community, *Rp* is *R. pseudoacacia*-dominated community, and *Ql* is *Q. liaotungensis*-dominated community

Table 7 Error matrix of different vegetation community types calculated using the VTI in the Chenjiagua and Shanghenian watersheds

	Bi	Ag	Hr	Rp	Ql	Total	Accuracy (%)
Chenjiagua watershed							
Bi	21	1	1	1	–	24	87.50
Ag	4	39	1	3	–	47	82.98
Hr	0	1	14	2	–	17	82.35
Rp	0	0	0	21	–	21	100.00
Ql	–	–	–	–	–	–	–
Total	25	41	16	27	–	109	
Overall accuracy (%)	87.16						
Overall kappa statistics	0.821						
Shanghenian watershed							
Bi	20	2	1	0	0	23	86.96
Ag	0	30	2	1	1	34	88.24
Hr	0	0	21	1	0	22	95.45
Rp	0	1	2	30	3	36	83.33
Ql	0	0	0	2	25	27	92.59
Total	20	33	26	34	29	142	
Overall accuracy (%)	88.73						
Overall kappa statistics	0.858						

Bi is B. ischaemum-dominated community, Ag is A. gmelinii-dominated community, Hr is H. rhamnoides-dominated community, Rp is R. pseudoacacia-dominated community, and Ql is Q. liaotungensis-dominated community

types at a 95 % confidence level using the Z test but the NDVI could not divide the availability of Bi and Ag ($Z=$ 1.95<1.96). The reason is that the NDVI is sensitive to atmospheric influence (Holben 1986); however, the VTI index uses shortwave infrared spectral bands (Landsat TM5 and TM7), wh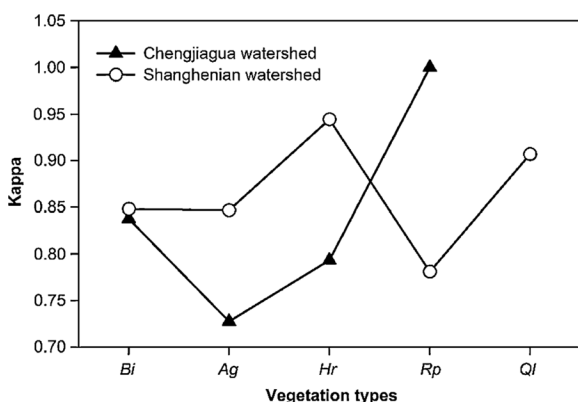ich are reported to be less influenced by aerosol interference (Karnieli et al. 2001; Kaufman et al. 1997; Qi et al. 2000; Tucker 1980). The TM image data in this study was processed using the MODTRAN 4 radiative transfer models to minimize the atmospheric influence. Meanwhile, the red band of the Landsat TM image data sets was used in generating the VTI because this wavelength's absorption by plant photosynthetic materials and pigments is maximal and the single-scattering approximation is more valid than that of the NIR (Chopping et al. 2003).

Table 11 shows the supervised classification accuracy of the five vegetation types using the MLC in the Chenjiagua and Shanghenian watersheds. The overall accuracy was 94.19 % for the Shanghenian watershed and 87.88 % for the Chenjiagua watershed with overall kappa statistics of 0.9301 and 0.8424, respectively. It indicated that the VTI has a similar accuracy with the supervised classification of MLC to detect the five vegetation types.

Fig. 10 Kappa statistics of the five vegetation community types in the two small watersheds. Bi is B. ischaemum-dominated community, Ag is A. gmelinii-dominated community, Hr is H. rhamnoides-dominated community, Rp is R. pseudoacacia-dominated community, and Ql is Q. liaotungensis-dominated community

Advantages of VTI over other VIs and methods

The VTI index detection of the five vegetation types on the Loess Plateau was dependent on the different

Table 8 Error matrix of different vegetation community types calculated using the VTI in the Landsat image (acquired date: August 12, 2007) and/or other regions outside the Yanhe watershed

	Bi	*Ag*	*Hr*	*Rp*	*Ql*	Total	Accuracy (%)	Kappa index
Bi	19	6	0	0	0	25	76.00	0.840
Ag	2	26	0	2	0	30	86.67	0.884
Hr	0	2	14	3	0	19	73.68	0.736
Rp	0	0	0	21	6	27	77.78	0.964
Ql	0	0	0	2	15	17	88.24	0.809
Total	21	34	14	28	21	118		
Overall accuracy (%)	80.51							
Overall kappa statistics	0.864							

Bi is *B. ischaemum*-dominated community, *Ag* is *A. gmelinii*-dominated community, *Hr* is *H. rhamnoides*-dominated community, *Rp* is *R. pseudoacacia*-dominated community, and *Ql* is *Q. liaotungensis*-dominated community

spectral characteristics in the TM3, TM5, and TM7 bands due to differences in chlorophyll and leaf water content. Previous studies on the Loess Plateau proved that the five vegetation types selected in this study had significant differences in chlorophyll and leaf water content ($p<0.05$) (An and ShangGuan 2007; Jin et al. 2008). Thus, the spectral reflectance of the five vegetation types was obviously distinguished due to the different absorptive abilities by chlorophyll in TM3 and by leaf water content in TM5 and TM7 (Jackson 1984; Jensen 2006). This provided the mechanism by which VTI could detect the five vegetation types effectively.

Compared with other vegetation indices or methods, although the VTI index was an empirical formula based on a larger regional scale and statistics with simple

Table 9 Error matrix of different vegetation community types calculated using the NDVI in the Chenjiagua and Shanghenian watersheds

	Other types	*Bi*	*Ag*	*Hr*	*Rp*	*Ql*	Total	Accuracy (%)	Kappa index
Chenjiagua watershed									
Bi	14	22	3	0	0	–	39	56.41	0.456
Ag	0	5	31	3	0	–	39	79.49	0.715
Hr	0	2	7	22	8	–	39	56.41	0.465
Rp	0	0	0	2	27	–	29	93.10	0.909
Ql	–	–	–	–	–	–	–	–	–
Total	14	29	41	27	35		146		
Overall accuracy (%)	69.86								
Overall kappa statistics	0.611								
Shanghenian watershed									
Bi	9	5	2	2	0	0	18	27.78	0.181
Ag	15	9	10	4	2	0	40	25.00	0.011
Hr	0	5	27	7	1	0	40	17.50	0.001
Rp	0	2	7	18	13	0	40	32.50	0.083
Ql	0	0	0	0	31	9	40	22.50	0.184
Total	24	21	46	31	47	9	178		
Overall accuracy (%)	24.72								
Overall kappa statistics	0.082								

Bi is *B. ischaemum*-dominated community, *Ag* is *A. gmelinii*-dominated community, *Hr* is *H. rhamnoides*-dominated community, *Rp* is *R. pseudoacacia*-dominated community, and *Ql* is *Q. liaotungensis*-dominated community

Table 10 Results of Z test for comparison between five vegetation types for NDVI and VTI

Comparison	Z statistic		Results[a]	
	NDVI	VTI	NDVI	VTI
Bi vs. *RP*	7.76	8.85	S	S
Bi vs. *Ql*	13.92	21.14	S	S
Bi vs. *Hr*	4.92	6.42	S	S
Bi vs. *Ag*	1.95	2.42	NS	S
Rp vs. *Ql*	2.05	6.49	S	S
Rp vs. *Hr*	2.50	4.01	S	S
Rp vs. *Ag*	5.67	7.18	S	S
Ql vs. *Hr*	5.28	13.41	S	S
Ql vs. *Ag*	10.11	18.41	S	S
Hr vs. *Ag*	2.99	4.10	S	S

Bi is *B. ischaemum*-dominated community, *Ag* is *A. gmelinii*-dominated community, *Hr* is *H. rhamnoides*-dominated community, *Rp* is *R. pseudoacacia*-dominated community, and *Ql* is *Q. liaotungensis*-dominated community

S significant, *NS* not significant

[a] At the 95 % confidence level

parameters, it has the advantage of expediently detecting vegetation types at a larger regional scale on the Loess Plateau. For example, the Poaceae abundance index (PAI), used to discriminate Poaceae grass from other plant spectral data in the semi-arid Mongolian steppes, was derived by combining four normalized difference indices: normalized green-blue difference index (NGBDI), normalized green-red difference index (NGRDI), NDVI, and normalized NIR-blue difference index (NNBDI) (Shimada et al. 2012). However, the

Table 11 Error matrix of different vegetation community types measured by supervised classification using the maximum likelihood classifiers in the Chenjiagua and Shanghenian watersheds

	Bi	*Rp*	*Ql*	*Hr*	*Ag*	Others	Total	Accuracy (%)
Shanghenian watershed								
Bi	17	0	0	0	0	0	17	100.00
Rp	0	30	0	2	0	0	32	93.75
Ql	0	0	27	0	0	0	27	100.00
Hr	1	0	0	26	2	0	29	89.66
Ag	3	0	0	0	22	0	25	88.00
Others	1	0	0	0	0	24	25	96.00
Total	22	30	27	28	24	24	155	
Overall accuracy (%)		94.19						
Overall kappa statistics		0.9301						
Chenjiagua watershed								
Bi	12	1	–	1	3	0	17	70.59
Rp	0	17	–	1	0	0	18	94.44
Ql	–	–	–	–	–	–	–	–
Hr	0	1	–	11	1	0	13	84.62
Ag	3	1	–	0	12	0	16	75.00
Others	0	0	–	0	0	35	35	100.00
Total	15	20	–	13	16	35	99	
Overall accuracy (%)		87.88						
Overall kappa statistics		0.8424						

Bi is *B. ischaemum*-dominated community, *Ag* is *A. gmelinii*-dominated community, *Hr* is *H. rhamnoides*-dominated community, *Rp* is *R. pseudoacacia*-dominated community, and *Ql* is *Q. liaotungensis*-dominated community

PAI was only tested at the quadrat scale. The inversion of the simple geometric model (SGM) of the surface bidirectional reflectance distribution function (BRDF) was developed to determine the grass and shrubs by the structural characteristics of different vegetation types in the Chihuahuan desert of the USA (Chopping et al. 2003); however, it required many parameters obtained from ground-based spectral data. Although those methods have been found to be effective at monitoring the vegetation types in their respective study regions, they are affected by scale and convenience in application. Moreover, comparison of VTI with NDVI showed that VTI was more sensitive in the monitoring of vegetation types than NDVI. The reason for this may be due to the sensitivity of NDVI in terms of atmospheric influence and soil background characteristics rather than VTI being developed by adding shortwave infrared bands which are more sensitive to vegetation senescence and less so to aerosol interference (Holben 1986; Karnieli et al. 2001; Kaufman et al. 1997; Qi et al. 2000). In addition, the maximum likelihood classification (MLC), as a pixel-based method, is most widely used in classifying remotely sensed data (Erener and Düzgün 2009; Huang et al. 2007; Shlien and Smith 1976). Numerous studies had shown that the MLC algorithm could obtain high precision and accuracy (Yang et al. 2011). However, it must calculate relevant parameters and determine the discriminant function for each category before classification (Erener 2013; Sun et al. 2013). This procedure will not only increase the time but also generate probable mistakes due to the inexperience of the classifier (Sun et al. 2013). Furthermore, for data with a non-normal distribution, the MLC results may be unsatisfactory (Erener 2013). The canonical discriminant analysis (CDA) is another method used for classification; however, spectral transformation by CDA uses coefficients obtained from class-related training samples and the transformation process involves human-*guided* effort and knowledge in selecting training samples (Guang and Maclean 2000). It has a similar limitation as the MLC. However, the VTI could overcome these limitations. The atmospheric correction before calculation of the VTI value of each vegetation type, based on the sensor features, was rapid. Furthermore, the classification basis of vegetation types was not dependent on the experience of a classifier. Meanwhile, the VTI also obtains satisfactory accuracy.

Conclusion

The traditional methods for detecting vegetation types involve intensive and time-consuming fieldwork and cannot be applied conveniently to large regions. Although the vegetation indices based on the remote sensing techniques are famous for the monitoring of vegetation information, there were no effective vegetation indices to detect vegetation types on the Loess Plateau area in China until now. In this study, a new method, the vegetation type index (VTI), was proposed to detect vegetation types based on the Landsat TM data. It was formed using two shortwave infrared bands (1.55–1.75 and 2.08–2.35 μm) and one visible band (0.63–0.69 μm) of Landsat TM image data. The VTI values clearly separated the five typical vegetation types including *B. ischaemum*-dominated, *A. gmelinii*-dominated, *H. rhamnoides*-dominated, *R. pseudoacacia*-dominated, and *Q. liaotungensis*-dominated communities on the Loess Plateau with satisfactory classification accuracy exceeding 85 % and kappa statistics above 0.8.

There is, however, still room for further improvement. Due to the low spatial resolution of Landsat TM data and the broken topography of the Loess hill-gully region, accurate detection of more vegetation types is still an open problem, which could be solved using image data from higher-spatial-resolution satellite instruments combined with field surveys. Furthermore, the research on the spectral reflection mechanism of different vegetation types using multi-spectral and hyperspectral remote sensing data and improving the accuracy of vegetation classification are important avenues for future research.

References

Adler-Golden, S.M., Matthew, M.W., Bernstein, L.S., Levine, R.Y., Berk, A., Richtsmeier, S.C., Acharya, P.K., Anderson, G.P., Felde, J.W., & Gardner, J. (1999). Atmospheric correction for shortwave spectral imagery based on MODTRAN4. In, *SPIE's International Symposium on Optical Science, Engineering, and Instrumentation* (pp. 61–69): International Society for Optics and Photonics.

An, H., & ShangGuan, Z.-P. (2007). Photosynthetic characteristics of dominant plant species at different succession stages of vegetation on Loess Plateau. *Chinese Journal of Applied Ecology, 18*, 1175–1180 (in Chinese with English abstract).

Carter, G. A., Lucas, K. L., Blossom, G. A., Lassitter, C. L., Holiday, D. M., Mooneyhan, D. S., Fastring, D. R., Holcombe, T. R., & Griffith, J. A. (2009). Remote sensing and mapping of tamarisk along the Colorado River, USA: a comparative use of summer-acquired Hyperion, Thematic Mapper and QuickBird data. *Remote Sensing, 1*, 318–329.

Chander, G., Markham, B. L., & Helder, D. L. (2009). Summary of current radiometric calibration coefficients for Landsat MSS, TM, ETM+, and EO-1 ALI sensors. *Remote Sensing of Environment, 113*, 893–903.

Chen, Y.-N., Ma, L.-S., Zhang, X.-R., Yang, J.-J., & An, S.-S. (2014). Ecological stoichiometry characteristics of leaf litter of *Robinia pseudoacacia* in the Loess Plateau of Shaanxi Province. *Acta Ecologica Sinica, 34*, 4412–4422 (in Chinese with English abstract).

Chopping, M. J., Rango, A., Havstad, K. M., Schiebe, F. R., Ritchie, J. C., Schmugge, T. J., French, A. N., Su, L., McKee, L., & Davis, M. R. (2003). Canopy attributes of desert grassland and transition communities derived from multiangular airborne imagery. *Remote Sensing of Environment, 85*, 339–354.

Congalton, R. G. (1991). A review of assessing the accuracy of classifications of remotely sensed data. *Remote Sensing of Environment, 37*, 35–46.

Dean, A. M., & Smith, G. M. (2003). An evaluation of per-parcel land cover mapping using maximum likelihood class probabilities. *International Journal of Remote Sensing, 24*, 2905–2920.

Duncan, J., Stow, D., Franklin, J., & Hope, A. (1993). Assessing the relationship between spectral vegetation indices and shrub cover in the Jornada Basin, New Mexico. *International Journal of Remote Sensing, 14*, 3395–3416.

Elmore, A. J., Mustard, J. F., Manning, S. J., & Lobell, D. B. (2000). Quantifying vegetation change in semiarid environments: precision and accuracy of spectral mixture analysis and the normalized difference vegetation index. *Remote Sensing of Environment, 73*, 87–102.

Erener, A. (2013). Classification method, spectral diversity, band combination and accuracy assessment evaluation for urban feature detection. *International Journal of Applied Earth Observation and Geoinformation, 21*, 397–408.

Erener, A., & Düzgün, H. S. (2009). A methodology for land use change detection of high resolution pan images based on texture analysis. *Italian Journal of Remote Sensing, 41*, 47–59.

Guang, Z., & Maclean, A. L. (2000). A comparison of canonical discriminant analysis and principal component analysis for spectral transformation. *Photogrammetric Engineering & Remote Sensing, 66*, 841–847.

Holben, B. (1986). Characteristics of maximum-value composite images from temporal AVHRR data. *International Journal of Remote Sensing, 7*, 1417–1434.

Hölzel, N., Buisson, E., & Dutoit, T. (2012). Species introduction—a major topic in vegetation restoration. *Applied Vegetation Science, 15*, 161–165.

Huang, X., Zhang, L., & Li, P. (2007). Classification and extraction of spatial features in urban areas using high-resolution multispectral imagery. *Geoscience and Remote Sensing Letters, IEEE, 4*, 260–264.

Huete, A. R. (1988). A soil-adjusted vegetation index (SAVI). *Remote Sensing of Environment, 25*, 295–309.

Jackson, R. D. (1984). Remote sensing of vegetation characteristics for farm management. *Remote Sensing: Critical Review of Technology, 475*, 81–96.

Jackson, R. D., & Huete, A. R. (1991). Interpreting vegetation indices. *Preventive Veterinary Medicine, 11*, 185–200.

Jensen, J. R. (2006). *Remote sensing of the environment: an earth resource perspective*. USA: Pearson Prentice Hall.

Jia, Y., Jiao, J., Wang, N., Zhang, Z., Bai, W., & Wen, Z. (2011). Soil thresholds for classification of vegetation types in abandoned cropland on the Loess Plateau, China. *Arid Land Research and Management, 25*, 150–163.

Jiao, J., Tzanopoulos, J., Xofis, P., & Mitchley, J. (2008a). Factors affecting distribution of vegetation types on abandoned cropland in the hilly-gullied Loess Plateau Region of China. *Pedosphere, 18*, 24–33.

Jiao, J., Zhang, Z., Jia, Y., Wang, N., & Bai, W. (2008b). Species composition and classification of natural vegetation in the abandoned lands of the hilly-gullied region of North Shaanxi Province. *Acta Ecologica Sinica, 28*, 2981–2997.

Jiao, F., Wen, Z.-M., & An, S.-S. (2011). Changes in soil properties across a chronosequence of vegetation restoration on the Loess Plateau of China. *Catena, 86*, 110–116.

Jin, T.-T., Liu, G.-H., Hu, C.-J., Su, C.-H., & Liu, Y. (2008). Characteristics of photosynthetic and transpiration of three common afforestation species in the Loess Plateau. *Acta Ecologica Sinica, 28*, 5758–5765.

Karnieli, A., Kaufman, Y. J., Remer, L., & Wald, A. (2001). AFRI—aerosol free vegetation index. *Remote Sensing of Environment, 77*, 10–21.

Kaufman, Y. J., & Tanre, D. (1992). Atmospherically resistant vegetation index (ARVI) for EOS-MODIS. *IEEE Transactions on Geoscience and Remote Sensing, 30*, 261–270.

Kaufman, Y. J., Wald, A. E., Remer, L. A., Gao, B. C., Li, R. R., & Flynn, L. (1997). The MODIS 2.1-μm channel-correlation with visible reflectance for use in remote sensing of aerosol. *IEEE Transactions on Geoscience and Remote Sensing, 35*, 1286–1298.

Li, D., Jiang, J., Liang, Y., Liu, G., & Huang, J. (1996). Study on water use efficiency of the artificial grassland at Ansai County in the Loess Hilly Region. *Research of Soil and Water Conservation, 3*, 66–74.

Major, D., Baret, F., & Guyot, G. (1990). A ratio vegetation index adjusted for soil brightness. *International Journal of Remote Sensing, 11*, 727–740.

Manandhar, R., Odeh, I., & Ancev, T. (2009). Improving the accuracy of land use and land cover classification of Landsat data using post-classification enhancement. *Remote Sensing, 1*, 330–344.

Nagase, A., & Dunnett, N. (2012). Amount of water runoff from different vegetation types on extensive green roofs: effects of plant species, diversity and plant structure. *Landscape and Urban Planning, 104*, 356–363.

Qi, J., Chehbouni, A., Huete, A., Kerr, Y., & Sorooshian, S. (1994). A modified soil adjusted vegetation index. *Remote Sensing of Environment, 48*, 119–126.

Qi, J., Marsett, R., & Heilman, P. (2000). Rangeland vegetation cover estimation from remotely sensed data. In, *Proceedings of the 2nd International Conference on Geospatial Information in Agriculture and Forestry* (pp. 243–252).

Qiu, L., Zhang, X., Cheng, J., & Yin, X. (2010). Effects of black locust (Robinia pseudoacacia) on soil properties in the loessial gully region of the Loess Plateau, China. *Plant and Soil, 332*, 207–217.

Sabins, F. F. (1987). Remote sensing principles and interpretation (2nd edn.). New York: Freeman.

Sakamoto, T., Wardlow, B. D., Gitelson, A. A., Verma, S. B., Suyker, A. E., & Arkebauer, T. J. (2010). A two-step filtering approach for detecting maize and soybean phenology with time-series MODIS data. *Remote Sensing of Environment, 114*, 2146–2159.

Shimada, S., Takahashi, H., & Limin, S. H. (2006). Hydroperiod and phenology prediction in a Central Kalimantan peat swamp forest by using MODIS data. *Tropics, 15*, 435–440.

Shimada, S., Matsumoto, J., Sekiyama, A., Aosier, B., & Yokohana, M. (2012). A new spectral index to detect Poaceae grass abundance in Mongolian grasslands. *Advances in Space Research, 50*, 1266–1273.

Shlien, S., & Smith, A. (1976). A rapid method to generate spectral theme classification of Landsat imagery. *Remote Sensing of Environment, 4*, 67–77.

Solutions, I.V.I. (2009). Atmospheric correction module: QUAC and FLAASH user's guide. In, *Boulder, CO: ITT Visual Information Solutions* (p. 44).

Su, C. H., Fu, B. J., Wei, Y. P., Lu, Y. H., Liu, G. H., Wang, D. L., Mao, K. B., & Feng, X. M. (2012). Ecosystem management based on ecosystem services and human activities: a case study in the Yanhe watershed. *Sustainability Science, 7*, 17–32.

Sun, J., Yang, J., Zhang, C., Yun, W., & Qu, J. (2013). Automatic remotely sensed image classification in a grid environment based on the maximum likelihood method. *Mathematical and Computer Modelling, 58*, 573–581.

Thomlinson, J. R., Bolstad, P. V., & Cohen, W. B. (1999). Coordinating methodologies for scaling landcover classifications from site-specific to global: steps toward validating global map products. *Remote Sensing of Environment, 70*, 16–28.

Thorne, K., Markharn, B., Barker, P. S., & Biggar, S. (1997). Radiometric calibration of Landsat. *Photogrammetric Engineering & Remote Sensing, 63*, 853–858.

Tucker, C. J. (1980). A critical review of remote sensing and other methods for non-destructive estimation of standing crop biomass. *Grass and Forage Science, 35*, 177–182.

van den Elsen, E., Hessel, R., Liu, B. Y., Trouwborst, K. O., Stolte, J., Ritsema, C. J., & Blijenberg, H. (2003). Discharge and sediment measurements at the outlet of a watershed on the Loess plateau of China. *Catena, 54*, 147–160.

Wang, L., Wei, S., Horton, R., & Shao, M. A. (2011). Effects of vegetation and slope aspect on water budget in the hill and gully region of the Loess Plateau of China. *Catena, 87*, 90–100.

Wen, Z., Lees, B. G., Jiao, F., Lei, W., & Shi, H. (2010). Stratified vegetation cover index: a new way to assess vegetation impact on soil erosion. *Catena, 83*, 87–93.

Xie, Y., Sha, Z., & Yu, M. (2008). Remote sensing imagery in vegetation mapping: a review. *Journal of Plant Ecology, 1*, 9–23.

Yang, C., Everitt, J. H., & Murden, D. (2011). Evaluating high resolution SPOT 5 satellite imagery for crop identification. *Computers and Electronics in Agriculture, 75*, 347–354.